Evaluation of uptake mechanisms of phosphate by Fe(III)(oxyhydr)oxides in Early Proterozoic oceanic conditions

Christoffer Hemmingsson, Iain K. Pitcairn, Ernest Chi Fru

Department of Geological Sciences, Stockholm University, SE-10691, Stockholm Sweden

*Correspondence and requests for materials should be addressed to:
christoffer.hemmingsson@geo.su.se

Additional keywords: DIP; Early Proterozoic; coprecipitation; adsorption; Iron formations

1. Introduction

Throughout earth's history, changing hydrothermal activity, continental weathering, redox and extreme climate regimes have influenced oceanic trace element content and oxidation state[1-6]. Early in Earth history, trace element contents in the ocean, particularly with respect to nutrients such as P, heavily influenced oceanic productivity, growth of cyanobacteria and the rise of oxygen production[7]. In modern day oceans phosphate availability is heavily influenced by its affinity for Fe(III) minerals as oxidation of aqueous Fe(II) to Fe(III)(oxyhydr)oxides binds and precipitates dissolved inorganic P (DIP), thereby controlling phosphate bioavailability[8-10]. The large-scale formation of banded iron formation (BIF) between ~2.5-1.8 Ga may have heavily influenced marine DIP concentrations at this time[2,7-11]. Early Proterozoic oceans are suggested to have been stratified with Fe(II)-rich (ferruginous) deep marine waters overlain by a shallow oxygenated ocean surface, following the permanent appearance of oxygen in the atmosphere at around 2.4-2.1 Ga[6,12]. Extensive precipitation of DIP by hydrothermal Fe(III)(oxyhydr)oxides in the water column followed by settling out and burial is suggested to have led to a nutrient-poor Early Proterozoic ocean, thereby affecting the growth of primary producers[7,11,13]. This has been suggested to have delayed oxygenation of the atmosphere and deep oceans until the Precambrian-Cambrian boundary when Fe(II) was titrated out of the oceans[2,6,7,11,14,]. This mechanism of DIP transfer referred to as the "Fe-shuttle" is driven by strong gradients in redox and chemical compositions in the Early Proterozoic ocean.

Marine DIP content during the Archean and Early Proterozoic is most commonly constrained through empirical models relating the adsorption of orthophosphate to Fe(III) (oxyhydr)oxides. These experimental models mimic Early Proterozoic seawater compositions using NaCl solutions containing elevated Si and Fe(II) and our understanding of P entrapment in Fe(III)(oxyhydr)oxides precipitated from the mixing of modern hydrothermal fluids with marine water[11,13,15,16]). The data can then be used to read the Early Proterozoic marine DIP record preserved as solid P in BIF[2,17]. Studies

investigating both adsorption and coprecipitation as mechanisms for incorporation of DIP into Fe(III)(oxyhydr)oxides have been carried out. Competitive adsorption measures attachment on surfaces of pre-formed natural or synthetic Fe(III)(oxyhydr)oxide minerals, while coprecipitation accounts for elemental concentrations incorporated into minerals that were grown in a solution where the ions coexist with Fe(II) and its oxidant. Adsorption measures the binding of dissolved ions to the surface of minerals that have already formed, analogous to minerals precipitated in shallow water sinking through the water column. Coprecipitation measures the ions incorporated into the mineral structure at the time of mineral growth. It remains unclear which of these two processes is the dominant enforcer of DIP removal from Early Proterozoic marine waters containing elevated Si and Fe(II). Without this assessment, it is difficult to determine whether the marine DIP record attained from BIF reflects the ocean conditions where the crystal grew (coprecipitation) or long-term scavenging of DIP by ageing Fe(III)(oxyhydr)oxide particles sinking from the photic, oxygenated surface zone to the aphotic anoxic ocean floor (adsorption).

This study quantifies DIP adsorption trends by pre-formed Fe(III)(oxyhydr)oxides in solutions equilibrated to seawater ionic strength of 0.56 M NaCl, and containing elevated Si and Fe(II) levels thought to reflect concentrations in open anoxic iron-rich bottom waters contacting the Early Proterozoic oxygenated ocean surface[2,6,14,18]. The results are compared with coprecipitation data produced under similar conditions, that showed significant scavenging of dissolved P by Fe(III)(oxyhydr)oxides grown in NaCl solution containing elevated Fe(II), Si, Mg^{2+}, Ca^{2+} and As[16]. The coprecipitation study also showed that the elevated As concentrations appear to negate the negative affect of high Si concentrations on P sorbtion(16). This study aims to investigate whether 1) coprecipitation of DIP by Fe(III)(oxyhydr)oxides resulting from the active oxidation of Fe(II) sourced from deep iron-rich open ocean waters is distinct from surface attachment of DIP during adsorption by pre-formed Fe(III)(oxyhydr)oxides, and 2) coprecipitation by Fe(III)(oxyhydr)oxides predominantly controlled DIP drawdown in Early Proterozoic open ocean surface waters where upwelling of deep anoxic iron (II)-rich waters mixed with the global thin sheet of oxic surficial waters[6]. This would imply that freshly formed Fe(III)(oxyhydr)oxides scavenged DIP from the oxic surface ocean, while attachment on the surfaces of Fe(III)(oxyhydr)oxides sinking to the bottom of the ocean was negligible. The magnitude of the difference between these two processes may enable insights into the

vertical distribution of DIP in the Early Proterozoic oceans, taking into account anoxic water column regeneration of DIP. Through mass balance calculations, we aim to evaluate whether ocean stratification following the permanent oxygenation of the atmosphere after 2.4 Ga changed vertical marine DIP dynamics.

2. Materials and methods

2.1. Mineral precipitation and adsorption experiments

Fifty-four individual Fe(III)(oxyhydr)oxide precipitates were synthesized from $FeCl_2*H_2O$ in ambient temperature and atmosphere, at circumneutral pH, close to the reconstructed pH of Precambrian waters[19]. A high Fe(II) concentration of 7.16 mM was selected for these precipitations to ensure enough surface area for adsorption and mineral analysis[20]. The precipitates were then used in a series of experiments investigating competitive adsorption between Si, P and As. The experiments were carried out at varying Si concentrations of 0.0, 0.67 and 2.2 mM ($Na_2O(SiO)_2x*xH_2O$), and across a pH range of 5-10. Equimolar concentrations of P and As to a total of 100 μM each were used to replicate conditions of a previous study[16], and a salinity of 0.56 M NaCl was used to mimic the conditions from other studies[13,15]. Fixed molar As/P ratios were used as varying the As:P ratio between 1:0.001 to 1:1000 has been shown to have no effect on P uptake by Fe(III)(oxyhydr)oxides[16], and furthermore, use of equimolar concentrations allows preferential ion uptake to be more clearly identified. The effects of Ca^{2+} and Mg^{2+} were not tested in this study because it has been shown that in the presence of As, these ions have no effect on the relationship between Si and P fixation by Fe(III)(oxyhydr)oxides[16]. Oxidation of As(III) during the experimental set up was not evaluated as it been shown during similar experimental conditions to be minimal (< 2%)[16]. The As concentration is similar to what would be expected in a hydrothermal plume with considerably higher metal contents than ambient seawater with estimated As concentrations in the Archean and Early Proterozoic of around 10 ppb[21]. The conditions of the adsorption experiments varied from previous studies[15], through addition of dissolved As(III), As(V) or a combination of these two As species with equimolar DIP for competitive adsorption. Precipitated material was washed three times in 0.56 M NaCl and immediately resuspended in a 0.56 M NaCl solution containing 100 μM of both P and As at the variable Si content and pH stated

above. The pH (5-10) was adjusted with 1 M NaOH or 1 M HCl solutions and maintained for 30 min of adsorption, after which a 1 ml sample was centrifuged for 7 min at 13 000 rpm. The 1 ml sample was then divided into supernatant that was filtered through 0.2 μm teflon filters and the remaining pellet (synthesized mineral, post-adsorption). Both the supernatant and pellet were dissolved in 2 ml 5% HNO_3 for Inductively Coupled Plasma-Optical Emission Spectroscopy (ICP-OES). A series of extra Fe(III)(oxyhydr)oxide precipitates were synthesized from $FeCl_2*H_2O$ at circumneutral pH with the addition of 0.67 and 2.2 mM $Na_2O(SiO)_2x*xH_2O$. These extra precipitates were synthesised in order to test the effects of Si on the mineralogy of the precipitates and to aid correlation with mineralogy in the previous coprecipitation study[16]. These extra precipitates were not used for elemental analysis nor the calculation of distribution coefficients.

2.2. Mineralogy of synthesized Fe(III)oxyhydr)oxides

Dried samples were gently crushed in agate mortar for analysis with environmental scanning electron microscopy (ESEM) in combination with electron dispersive spectroscopy (EDS) to check sample homogeneity and to collect initial qualitative elemental data. Powder x-ray diffraction (PXRD) analysis to characterise mineralogical composition was carried out at the Swedish Museum of Natural history using an Analytical Xpert-pro diffractometer at room temperature. Samples were run at 45 kV and 40 mA, with a step size of 0.017° and scan step time 50.1650 s, with continuous scanning of a rotating sample using Cu-Kα radiation and Ni-filter. Rough mineral quantification was performed with the Rietveld method to estimate relative mineral abundances in weight %. The mineral proportions were calculated using Rietveld analyses and the assumption of a 100% precipitation rate using the formulas of 2-line Ferrihydrite ($Fe_2O_3*0.5H_2O$), Lepidocrocite (FeOOH), and Magnetite (Fe_3O_4). The concentrations of P and As bound to each mineral were normalised to a sample weight of 1 g. The surface area for each mineral, (600, 80 and 90 m^2g^{-1} respectively[22-24]), was used to estimate the surface area available during adsorption compared to coprecipitation based on surface area per gram mineral.

Further mineralogical confirmation using Raman spectroscopy was carried out at the Department of Geological Sciences, Stockholm University, using a Horiba LabRAM HR 800 with a multichannel air-cooled (-70°C) CCD (charge-coupled device) array detector with 1024 x 256 pixels with spectral resolution ~0.3 cm^{-1}/pixel. The instrument was coupled

to a confocal Olympus BX41 microscope with laser beam focused through an 80x objective at 8 mm working distance with resulting spot size ~1 μm and laser power of 0.15 to 0.06 mW optimal for samples sensitive to transformation. Instrument accuracy was controlled by repeated use of a Silicon wafer calibration and the Raman spectra were collected with LabSpec 5 software.

Elemental analyses of the filtrate and supernatant from the adsorption experiments were carried out using a Thermo ICAP 6500 Duo ICP-OES with a concentric spray chamber and a V-groove nebuliser at the Department of Geological Sciences, Stockholm University. Precision and error were controlled through repeated analyses of external reference material NIST 1640a and use of an internal standard solution (Y1) to control drift. Detection limits for As, Fe, P, and Si are 2.49, 0.13, 0.74, and 0.28 ppb, respectively. Due to difficulties resulting from the ionization of excess Na remaining in solution, the concentration of P and As in the supernatants were calculated by subtracting the amount bound by Fe(III)(oxyhydr)oxide sample pellets from the initial solution concentrations.

2.3. P adsorption distribution coefficients (Kd)

The Kd for P was derived following methods described in previous studies[8,11,15,16] by plotting molar P/Fe in the Fe(III)(oxyhydr)oxides against DIP remaining in solution at each pH and Si concentration, using the equation $[P_d]=(1/K_{ads})(P_{ads}/Fe^{3+})$, where $[P_d]$ is dissolved P in solution, K_{ads} is the distribution coefficient from adsorption (referred to as Kd in this study), and (P_{ads}/Fe^{3+}) is the P/Fe ratio of Fe(III)(oxyhydr)oxide[11]. The Kd is essentially the slope of the linear correlation between P/Fe molar ratios in Fe(III)(oxyhydr)oxides particles against DIP given in the equation as $[P_d]$. The comparison between calculated adsorption Kds from this study are compared with coprecipitation Kd values from Chi Fru et al. (2016) to distinguish whether adsorption or coprecipitation controls P-uptake during Fe(III)(oxyhydr)oxide formation.

3. Results

3.1. Characterization of synthesized Fe(III)(oxyhydr)oxide minerals

The PXRD analyses show that the Fe(III)(oxyhydr)oxide precipitates used for the adsorption experiments contain multiple mineral phases, namely 2-line ferrihydrite,

lepidocrocite, magnetite and halite (Fig. 1). The Raman spectroscopy also confirmed the presence of 2-line ferrihydrite, lepidocrocite and magnetite (Fig. 2). Rietveld analysis of PXRD spectra indicates that the starting material contained 28% 2-line ferrihydrite, 71% lepidocrocite and 1% magnetite (Table 1), and that the relative abundances of minerals changed during the adsorption experiments. In general, lepidocrocite decreased and magnetite increased in abundance during the experiments (Table 1), and 2-line ferrihydrite increased in abundance in most of the adsorption experiments compared to the composition of the starting material (Fig. 1, Table 1). Rietveld analysis performed on PXRD spectra from Chi Fru et al. (2016), indicate that the precipitates generated in that study were pure 2-line ferrihydrite (Table 1). The extra Fe(III)(oxyhydr)oxide precipitates synthesized from solutions containing different concentrations of dissolved Si show that increasing dissolved Si concentrations during precipitation promotes the synthesis of 2-line ferrihydrite, with 2-line ferrihydrite and magnetite being the only Fe(III)(oxyhydr)oxide phases precipitated at the highest Si concentration (Fig. 3, 4)

3.2 Adsorption of P on Fe(III)(oxyhydr)oxide minerals

ICP-OES data suggest that DIP adsorption was pH dependent (Fig. 5a-i). At low pH, higher levels of DIP are adsorbed to the surface of the Fe(III)(oxyhydr)oxides, before rapidly dropping off to near zero as pH increases to 10. The adsorption of DIP was also affected by Si concentration, decreasing with increased Si in solution (Fig 5a-i). This occurred irrespective of the valency of As in solution. The adsorption of DIP is greater than that of As(V) at all pH and Si concentrations (Fig. 5d-f). Adsorption of As(V) shows similar behaviour to DIP, decreasing with increasing pH and dissolved Si (Fig. 5d-f). The adsorption of As(III) increases with increasing pH to values of around 7-8 (Fig. 5a-c). At pH > 8 As(III) adsorption remains constant in the Si free solution but decreases when Si is present (Fig. 5a-c). The experiments show that greater amounts of As(III) are adsorbed than As(V). Adsorption of DIP coexisting with As(III) and As(V) revealed a mixed pattern with characteristics of both the individual As(III) and As(V) trends, where As(V) is likely adsorbed to a higher degree at low pH and As(III) at high pH (Fig. 5g-i).

The average adsorption Kd value calculated across the pH range of 5-10 at the three concentrations of Si is ~0.0002 μM^{-1} (Fig. 6). Although the Kd varies somewhat with pH, this variation is not statistically significant (Table 2).

4. Discussion

4.1 Mineralogy and composition of Fe(III)(oxyhydr)oxide precipitates

The Fe(III)(oxyhydr)oxide precipitates synthesized in this study comprise multiple mineral phases with the starting material containing 28% 2-line ferrihydrite, 71% lepidocrocite and 1% magnetite (Table 1), which is distinct from the pure 2-line ferrihydrite produced in the coprecipitation experiments[16]. The different mineralogy synthesized in each study could be driven by the As, P, Ca or Mg content as these ions were present in the Fe(III)(oxyhydr)oxide precipitation solutions in the coprecipitation experiments, but not in the adsorption experiments reported here. Pure 2-line ferrihydrite was synthesized during coprecipitation in the previous study[16] despite variation of dissolved Si suggesting that Si content was not the only control on the different mineralogies produced in the 2 studies (Table 1). In the adsorption experiments reported here, lepidocrocite decreases in abundance from the starting material irrespective of the Si content indicating that the Si content of the adsorption solutions does not control its stability. The Si content however, does appear to exert control on the stability of ferrihydrite, which increases in abundance in the extra precipitations carried out in the presence of dissolved Si (Figs. 3 and 4). This is in agreement with earlier studies where solutions with Si/Fe ratio <0.1, yielded mainly lepidocrocite during rapid oxidation of Fe(II), whereas those with Si/Fe ratios >0.36 preferentially generated ferrihydrite[27,28]. With the decrease in the relative abundance of lepidocrocite during the adsorption experiments reported here, follows an increase in the abundance of magnetite and to a lesser degree, 2-line ferrihydrite (Table 1). The presence of magnetite may be explained by the decomposition of 2-line ferrihydrite[29], although this reaction is suggested to require reducing conditions and is commonly accompanied by dissimilatory reduction of 2-line ferrihydrite. Regardless of the reasons for the formation of magnetite, its presence is useful for this study as the increased number of mineral species to some degree mimics natural systems where multiple Fe(III)(oxyhydr)oxides are

common[22-24]. The presence of different solutes during Fe(II) oxidation most likely drives production of Fe(III)(oxyhydr)oxides with different degrees of purity.

The surface area available for trace metal attachment on synthetic lepidocrocite, 2-line ferrihydrite and magnetite are distinctly different, averaging ~80 m^2 g^{-1}, 600 m^2 g^{-1}, and 90 m^2 g^{-1} respectively[22-24]. This highlights the importance of the mineral assemblage as it affects the adsorptive capacity, particularly when 2-line ferrihydrite is present. With the formation of lepidocrocite and magnetite, the total adsorption capacity of competing phosphate, As(V) and As(III) ions would therefore be substantially reduced compared to when 2-line ferrihydrite is more abundant. For example, adsorption potential of phosphate at pH 7 on 2-line ferrihydrite, lepidocrocite and magnetite is 1037.55, 123.82 and 34.56 µmol g^{-1} respectively[30]. The greatly higher P adsorption potential of 2-line ferrihydrite[30] means that this mineral controls the P sorption in this study (Table 1). The effect of the lower abundance of 2-line ferrihydrite can be evaluated through calculation of hypothetical concentrations of adsorbed P, assuming 100% 2-line ferrihydrite and that P adsorption is proportional to the 2-line ferrihydrite abundance. The P adsorbed, assuming a hypothetical 100% 2-line ferrihydrite in adsorption experiments, would be between 2 and 6 times higher than that measured with the mixed mineralogy (Table 1). However, these hypothetical values are still considerably lower than the levels of P sorption during coprecipitation[16], varying from 2 to 49% (average 19%) of P incorporated during coprecipitation[16] (Table 1).

4.2 Competitive adsorption onto Fe(III)(oxyhydr)oxide and the role of As

One of the key results from this study is the relative differences in adsorption behaviour between P, As(III), and As(V). As(V) is adsorbed to a lesser degree than P but shows similar behaviour with adsorption decreasing with increasing pH as expected (Dixit and Hering, 2003). As(III) shows a distinctly different behaviour to P and As(V) with adsorption increasing as pH increases up to pH 7-8, and either remaining constant or decreasing between pH 8 and 10. The pH-dependent As(III) trend is also consistent with previous studies[23]). The different adsorption behaviour of P and As(III) with increasing pH may partially be explained by the change in surface charge of Fe(III)(oxyhydr)oxides with pH. The charge is positive at low pH, but reverses at pH 7 becoming progressively negative as pH increases[31]. Our experiments show a change from DIP to As(III)-favoured

adsorption at around pH 6-7 (Fig. 5a-c). The decreasing adsorption of P and As(V) with increasing pH (with consistently higher absorption of P than As(V)) (Fig. 5d-f), support previous studies that show that increasing DIP content reduces total As adsorption on Fe(III)(oxyhydr)oxides[32]. The results from the combined As(III)-As(V) experiments appear to show a mix of the results of the independent As(III) and As(V) reactions (Fig. 5g-i), pointing to presence of different types of adsorption sites on the mineral surface, favouring one valence state over the other.

Our results also show that P adsorption decreases with increasing Si content regardless of As speciation. This is in line with previous adsorption experiments[15], but contrasts strongly with behaviour during coprecipitation experiments where the effect of Si on P incorporation is muted when As is present in solution[16]. Such different behaviour suggests different DIP fixation mechanisms during coprecipitation and adsorption. Both coprecipitation and adsorption studies show that binding of As(III) and P occurs on different attachment sites while P and As(V) compete for similar attachment sites[33]. This explains the higher content of As(III) than As (V) as DIP occupies some of the As(V) binding sites. Coprecipitation samples[16] on the other hand have less mineralogical diversity than adsorption samples with a higher proportion of 2-line ferrihydrite and therefore a greater reactive surface area and ability to scavenge P and As from a water column. On average, ~5% of P and ~10% of As is removed via adsorption as opposed to coprecipitation although this increases to 19% and 42% using the hypothetical adsorption values calculated for a mineralogy of 100% FeH. The adsorption capacity of the samples in this study is clearly lowered by the mixed mineralogy (Table 1). As discussed above however, even if the P adsorbed is normalised to 100% 2-line ferrihydrite, the values are significantly less than P incorporated into 2-line ferrihydrite during coprecipitation[16]. The calculated average P adsorption Kd of 0.0002 μM^{-1} is very low compared to 0.072 μM^{-1} obtained for coprecipitation[16].

4.3. Implications on Early Proterozoic marine P and As cycling

Much of our understanding of marine P systematics in the Early Proterozoic comes from our knowledge of how this element behaves in the modern ocean, where P input is dominated by terrestrial weathering with inorganic P divided into DIP and particulate

inorganic phosphorus (PIP) (apatite and P bound by iron-manganese(oxyhydr)oxides), transported via rivers. The PIP isn't accessible for marine biota but sinks and deposits on continental shelves and in estuaries[34], and of the total P input only 10-30% is estimated to be available for biological uptake. Dissolved phosphate is an essential micronutrient incorporated into planktonic life living in surface waters and remineralized at deeper water depths. Fe(III)(oxyhydr)oxides are the major sedimentary sink for DIP[8,9,35-401] and can account for up to ~33% of total P buried in iron-rich hydrothermal sediments[3]. Fe(III)(oxyhydr)oxide precipitates formed in active hydrothermal plumes in the deep ocean contain abundant P scavenged from the water column with the Fe/P ratio of the precipitates being a function of the DIP of the oceanic water[8]. Some of the initial P bound by Fe(III)(oxyhydr)oxides, perhaps as much as 50% according to some studies[8,11], may be released during diagenesis due to transition from ferrihydrite to goethite[3] or dissimilatory iron reduction (DIR) of Fe(III)(oxyhydr)oxides by respiratory bacteria[42], a process which is thought to have been active since the Archean[43,44].

Oceanic conditions in the Early Proterozoic would have differed significantly from those of the modern day with the deep oceans being generally anoxic[45], ferruginous[14], silicic[46] and enriched in trace elements including Ni, Co, Au, As, Mn, Ba produced from more extensive hydrothermal plume activity at the time[21]. As well as anoxic deep ocean water, two other main redox environments are generally accepted to have been present in the Archean and Early Proterozoic oceans; oxic surface waters and sulphur rich euxinic conditions occurring proximal to continental margins[47]. Trace element input to the Early Proterozoic oceans would have occurred through hydrothermal activity and also through continental weathering, which most likely provided considerable input of nutrients including C and P[47,48]. It has been recently proposed that the DIP content of the Early Proterozoic oceans varied both on local and global scales, depending on the immediate influence of hydrothermal activity and weathering fluxes of P and As[16,49]. Our results support this observation as they indicate considerable variation of DIP content in the oxic, sulfidic and ferruginous areas of the Early Proterozoic oceans (Figs 8 and 9). Locally, DIP may have been more abundant in the sulfide-rich continental margins dominated by Fe-sulfide rather than Fe(III)(oxyhydr)oxides deposition, as sulfides do not scavenge P. Oxic surface waters where Fe(III)(oxyhydr)oxides form would become depleted in DIP due to coprecipitation[16]

and adsorption processes. The Fe(III)(oxyhydr)oxides produced in the oxic layer also have the potential to affect the deeper ocean chemistry as they settle through the water column. High dissolved Si content in the deeper ocean waters of pH values around 8 would inhibit P adsorption by ageing Fe(III)(oxyhydr)oxides (Fig. 7a) settling from the photic zone. However release of P into bottom waters is likely to have occurred during breakdown of Fe(III)(oxyhydr)oxides during diagenesis. Consequently, the long-term continuous delivery of P by Fe(III)(oxyhydr)oxides to the bottom waters would have increased DIP in the deep ocean. Scavenging of P by Fe(III)(oxyhydr)oxides at depth would have been minimal relative to the surface ocean where rapid large scale P fixation by coprecipitation would have occurred during growth of Fe(III)(oxyhydr)oxides[16]. This suggests that coprecipitation rather than surface adsorption on ageing Fe(III)(oxyhydr)oxides is the major pathway for P removal in seawater[3,39,40,50].

Surface waters would also become relatively enriched in As(V), the stable form of As in oxic environments, as P is preferentially incorporated into Fe(III)(oxyhydr)oxides over As (V) during coprecipitation and adsorption (Fig. 5d-f). This would therefore increase the possibility of As(V) toxicity and P-limitation in surface waters, compared to the broadly anoxic deeper ocean water column (Fig. 8a-b). We propose that Fe(III)(oxyhydr)oxide precipitation at the ferruginous/oxic surface boundary could have in the long-term caused a P famine in the oxic/photic zone of the Early Proterozoic open oceans, whilst also enriching the surface ocean in As(V). The dissolved As(V)/P molar ratios most likely affected the long-term bioavailability of P to primary producers in the photic zone[51-54] and therefore the long term production of O_2[16,55].

5. Conclusions

This study investigated the relative effectiveness of adsorption and coprecipitation on the uptake of DIP by Fe(III)(oxyhydr)oxides. Experiments were conducted in solutions formulated to mimic Early Proterozoic seawater with elevated levels of Si, Fe and As. Our results show that coprecipitation is considerably more effective than adsorption at removing DIP from the experimental solutions. Adsorption removes an average of 4% of the DIP removed by coprecipitation, increasing to 19% had the mineralogy been pure

ferrihydrite. Our results are in line with previous adsorption experiments that show that DIP uptake is limited by increased dissolved Si[15]. Uptake of DIP by coprecipitation is however, in the presence of dissolved As, not affected by the dissolved Si content and is therefore an effective process for removing DIP from the surface waters of the Early Proterozoic oceans[16]. The continuous shuttling of Fe(III)(oxyhydr)oxides would create localised P famine in surface waters meanwhile enriching the deep waters in DIP. Selective adsorption of DIP over As may have led to As(V) enrichment in surface waters which, combined with the limited availability of DIP, could have decreased productivity and ultimately contributed to delayed oxygenation of the upper oceans and atmosphere. Deep waters may have become enriched in DIP over time as some of the DIP shuttled into the anoxic deeper water and sediments is released due to recrystallisation of Fe(III)(oxyhydr)oxides over time, highlighting the possibility of DIP stratification in the Early Proterozoic oceans.

Acknowledgements

We would like to thank Magnus Mörth for the ICP-OES analysis and Curt Broman for the Raman analysis at Stockholm University. This project was funded by grant No. 336092 from the European Research Council.

Conflicts of interest

The authors declare no conflicts of interest

References

[1] D.E. Canfield, A new model for Proterozoic ocean chemistry. *Nature.* **1998**, 396, 450-453.

[2] A. Bekker, J.F. Slack, N. Planavsky, B. Krapež, A. Hofmann, K.O. Konhauser, O.J. Rouxel, Iron formation: the sedimentary product of a complex interplay among mantle, tectonic, oceanic, and biospheric processes. *Econ. geol.* **2010,** 105, 467-508.

[3] S.W. Poulton, D.E. Canfield, Co-diagenesis of iron and phosphorus in hydrothermal sediments from the southern East Pacific Rise: Implications for the evaluation of paleoseawater phosphate concentrations. *Geochim. Cosmo. Acta.* **2006***,* 70, 5883–5898.

[4] C.T. Reinhard, N.J. Planavsky, L.J. Robbins, C.A. Partin, B.C. Gill, S.V. Lalonde, A. Bekker, K.O Konhauser, T.W. Lyons, Proterozoic ocean redox and biogeochemical stasis. *Proc. Natl. Acad. Sci. U.S.A.* **2013**, 110, 5357-5362.

[5] F. Horton, Did phosphorus derived from the weathering of large igneous provinces fertilize the Neoproterozoic ocean?. *Geochem. Geophy. Geosyst*. **2015**, 16, 1723-1738.

[6] T.W. Lyons, C.T. Reinhard, N.J. Planavsky, The rise of oxygen in Earth's Early Ocean and atmosphere. *Nature.* **2014***,* 506, 307-315.

[7] C.T. Reinhard, N.J. Planavsky, B.C. Gill, K. Ozaki, L.J. Robbins, T.W. Lyons, W.W. Fischer, C. Wang, D.B. Cole, K.O. Konhauser, Evolution of the global phosphorus cycle. *Nature***. 2017,** 541, 386–389.

[8] R.A. Feely, J.H. Trefry, G.T. Lebon, C.R. German, The relationship between P/Fe and V/Fe ratios in hydrothermal precipitates and dissolved phosphate in seawater. *Geophy. Res. lett.* **1998**, 25, 2253-2256.

[9] T. Schaller, J. Morford, S.R. Emerson, R.A. Feely, Oxyanions in metalliferous sediments: Tracers for paleoseawater metal concentrations?. *Geochim. Cosmo. Acta.* **2000***,* 63, 2243-2254.

[10] J.A. Hawkee, D.P. Connelly, M.J.A. Rijkenberg, E.P. Achterberg, The importance of shallow hydrothermal island arc systems in ocean biogeochemistry. *Geophy. Res. Lett.* **2014**, 41, 942-947.

[11] C.J. Bjerrum, D.E. Canfield, Ocean productivity before about 1.9 Gyr limited by phosphorus adsorption onto iron oxides. *Nature.* **2002,** 417, 159-162.

[12] O.J. Rouxel, A. Bekker, K.J. Edwards, Iron isotope constraints on the Archean and Paleoproterozoic ocean redox state. *Science.* **2005***,* 307, 1088-1091.

[13] C. Jones, S. Nomosatryo, C.J. Bjerrum, D.E Canfield, Iron oxides, divalent cations, silica, and the early earth phosphorus crisis. *Geology.* **2015**, 43, 135-138.

[14] S.W. Poulton, D.E. Canfield, Ferruginous conditions: A dominant feature of the ocean through Earth's history. *Elements.* **2011***,* 7, 107-112.

[15] K.O. Konhauser, S.V. Lalonde, L. Amskold, H.D. Holland, Was there really an Archean Phosphate Crisis?. *Science.* ***2007,*** 315,1234.

[16] E. Chi Fru, C. Hemmingsson, M. Holm, B. Chiu, E. Iñiguez, Arsenic-induced phosphate limitation under experimental Early Proterozoic oceanic conditions. *Earth plan. sci. lett*. **2016**, 434, 52-63.

[17] (a) N.J. Planavsky, O.J. Rouxel, A. Bekker, S.V. Lalonde, K.O. Konhauser, C.T. Reinhard, T.W. Lyons, The evolution of the marine phosphate reservoir. *Nature.* **2010***,* 467, 1088-1090.

[18] N. Planavsky, O.J. Rouxel, A. Bekker, A. Hoffman, C.T.S. Little, T.W. Lyons, Iron isotope composition of some Archean and Proterozoic iron formations. *Geochim. cosmo. Acta.* **2012**, 80**,** 158-169.

[19] I. Halevy, A. Bachan, The geologic history of seawater pH. *Science.* ***2017,*** 355, 1069–171.

[20] M.W. Bligh, T.D. Waite, Formation, reactivity, and ageing of ferric oxide particles formed from Fe(II) and Fe(III) sources: implications for iron bioavailability in the marine environment. *Geochim. Cosmochim. Acta.* **2011,** 75, 7741-7758.

[21] R.R. Large, I. Mukherjee, D.D. Gregory, J.A. Steadman, V.V. Maslennikov, S. Meffre, Ocean and Atmosphere Geochemical Proxies Derived from Trace Elements in Marine Pyrite: Implications for Ore Genesis in Sedimentary Basins. *Economic Geology.* **2017***,* 112, 423-450.

[22] S. Choi, S. Hong, E.R. Baumann, Adsorption of Ferrous iron on the lepidocrocite surface. *Environ. Technol*. **2001**, 22*,* 355-365.

[23] S. Dixit, J.G. Hering, Comparison of arsenic(V) and arsenic(III) sorption onto iron oxide minerals: implications for arsenic mobility. *Environ. Sci. Technol.* **2003**, 37, 4182-4189.

[24] U. Schwertmann, R.M. Cornell, Iron oxides in the laboratory. Preparation and characterization. Second, completely revised and extended edition. **2008**, (Wiley-VCH).

[25] K. Müller, V.S.T. Ciminelli, M.S.S Dantas, S. Willscher, A Comparative study of As(III) and As(V) in aqueous solutions and adsorbed on iron oxy-hydroxides by raman spectroscopy. *Water research.* **2010***,* 44, 5660-5672.

[26] S. Das, M.J. Hendry, Application of raman spectroscopy to identify iron minerals commonly found in mine wastes. *Chemical geology.* **2011***,* 290, 101-108.

[27] T.D. Mayer, W.M. Jarrell, Formation and stability of iron(II) oxidation products under natural concentrations in dissolved silica. *Wat. Res.* **1996**, 5, 1208-1214.

[28] S. Bang, X. Meng, A review of arsenic interactions with anions and iron hydroxides. *Environ. Eng. Res.* **2004**, 9, 184-192.

[29] A. Zegeye, S. Bonneville, L.G. Henning, A. Sturm, D.A. Bowle, C. Jones C, D.E. Canfield, C. Ruby, L.C. MacLean, S. Nomosatryo, S.A. Crowe, S.W. Poulton, Green rust

formation controls nutrient availability in a ferruginous water column. *Geology.* **2012***,* 40, 599-602.

[30] T. Barber, Phosphate adsorption by mixed and reduced iron phases in static and dynamic systems, MSc thesis, Stanford University, 2002.

[31] J. Wan, S. Simon, V. Deluchat, M. Dictor, C. Dagot, Adsorption of As(III), As(V) and dimethylarsinic acid onto synthesized lepidocrocite. *J. Environ. Sci. health. Part.* **2013**, 48, 1272-1279.

[32] S.R. Chowdhury, E.K. Yanful, Arsenic and chromium removal by mixed magnetite-maghemite nanoparticles and the effect of phosphate on removal. *J. Environ. Management.* **2010,** *91*, 2238-2247.

[33] H. Zeng, B. Fisher, D.E. Glammar, Individual and competitive adsorption of arsenate and phosphate to a high-surface-area iron oxide-based sorbent. Environ. *Sci. Technol.* **2008**, 42, 147-152.

[34] A. Paytan, K. McLaughlin, The oceanic phosphorus cycle. *Chem. Rev.* **2007**, 107, 563–576.

[35] S. Matijević, Z. Kljaković-Gašpić, D. Bogner, A. Gugić, D. Marintovićartinovic, Vertical distribution of phosphorus species and iron in sediment at open sea stations in the Adriatic region. *Acta adriatica.* **2008***,* 49, 165-184.

[36] H.S. Jensen, P.B. Mortensen, F. Ø. Andersen, E.K. Rasmussen, A. Jensen, Phosphorus cycling in coastal marine sediment. *Limnol. Oceanogr.* **1995**, 40, 908-917.

[37] C.P. Slomp, E.H. Epping, G.W. Helder, W. van Raaphorst, A key role for iron-bound phosphorus in authigenic apatite formation in North Atlantic continental platform sediments. *J. Mar. Res*. **1996**, 54, 1179-1205.

[38] P. Anshutz, S. Zhong, B. Sundby, Burial efficiency of phosphorus and the geochemistry of iron in continental margin sediments, *Limnol. Oceanogr.* **1998,** 43, 53-64.

[39] R.A. Feely, G.J. Massoth, E.T. Baker, G.T. Lebon, T. Geiselman, Tracking the dispersal of hydrothermal plumes from the Juan de Fuca Ridge using suspended matter compositions. *J. Geophys. Res.* **1992**, 97, 3457–3468.

[40] R.A. Feely, G.J. Massoth, J.H. Trefry, E.T. Baker, A.J. Paulson, G.T. Lebon, Composition and sedimentation of hydrothermal plume particles from North Cleft segment, Juan de Fuca Ridge. *J. Geophys. Res.* **1994**, 99, 4985–5006.

[41] P. Lopez, Spatial distribution of sedimentary P pools in a Mediterranean coastal lagoon 'Albufera d'es Grau' (Minorca Island, Spain). *Mar. Geol.* **2004**, 203, 161-176.

[42] K.A. Weber, L.A. Achenbach, J.D. Coates, Microorganisms pumping iron: anaerobic microbial iron oxidation and reduction. *Nat. Rev. Microbiol.* **2006**, 4, 752-764.

[43] C.M. Johnson, B.L. Beard, E.E. Roden, The iron isotope fingerprints of redox and biogeochemical cycling in modern and ancient Earth. *Annual Rev Earth Plan. Sci*. **2008**, 36, 457-493.

[44] P.R. Craddock, N. Dauphas, Iron and carbon isotope evidence for microbial iron respiration throughout the Archean. *Earth plan. sci. lett.* **2011**, 303, 121-132.

[45] H.D. Holland The chemical evolution of the atmosphere and oceans. **1984**, 598. Princeton University Press.

[46] R. Siever, The silica cycle in the Precambrian. *Geochimi. Cosmo. Acta*. **1992**, 56, 3265-3272.

[47] S.W. Poulton, P.W. Fralick, D.E. Canfield, Spatial variability in oceanic redox structure 1.8 billion years ago. *Nature Geosci.* **2010**, 3, 486–490.

[48] J.A. Baross, S.E. Hoffman, Submarine hydrothermal vents and associated gradient environments as sites for the origin and evolution of life, *Origins of life,* **1985**, 15, 327-345.

[49] C.R. German, A.C. Campbell, J.M. Edmond, Hydrothermal scavenging at the Mid-Atlantic Ridge: modification of trace element dissolved fluxes. *Earth Planet. Sci. Lett.* **1991**, 107, 101–114.

[50] L.R. Kump, W.E. Seyfried, Hydrothermal Fe fluxes during the Precambrian: effect of low oceanic sulfate concentrations and low hydrostatic pressure on the composition of black smokers. *Earth Planet. Sci. Lett.* **2005**, 235, 654–662.

[51] G.A. Cutter, L.S. Cutter, Biogeochemistry of arsenic and antimony in the North Pacific Ocean. *Geochem. Geophy. Geosyst.* **2006**, 7, doi: 10.1029/2005GC001159.

[52] S.T. Dyhrman, S.T. Haley, Arsenic resistance in the unicellular marine diazotroph *Crocosphaera Watsonii*. *Front. Microbiol.* **2011**, 2, 214. doi: 10.3389/fmicb.2011.00214.

[53] O. Curl, L. Zimmer, G.A. Cutter, Arsenic and phosphorus biogeochemistry in the ocean: Arsenic species as proxies for P-limitation. *Limnol. Oceanogr.* **2013**, 58, 729-740.

[54] M. Elias, A. Wellner, K. Goldin-Azulay, E. Chabriere, J.A. Vorholt, T.J. Erb, D.S. Tawfik, The molecular basis of phosphate discrimination in arsenate-rich environments. *Nature.* **2012**, 491,134-7.

[55] E. Chi Fru, N. Arvestål, N. Callac, A. El Albani, S. Kilias, A. Argyraki, M. Jakobsson, Arsenic stress after the Proterozoic glaciations. *Sci. Rep.* **2015**, 5, 17789 doi: 10.1038/srep17789.

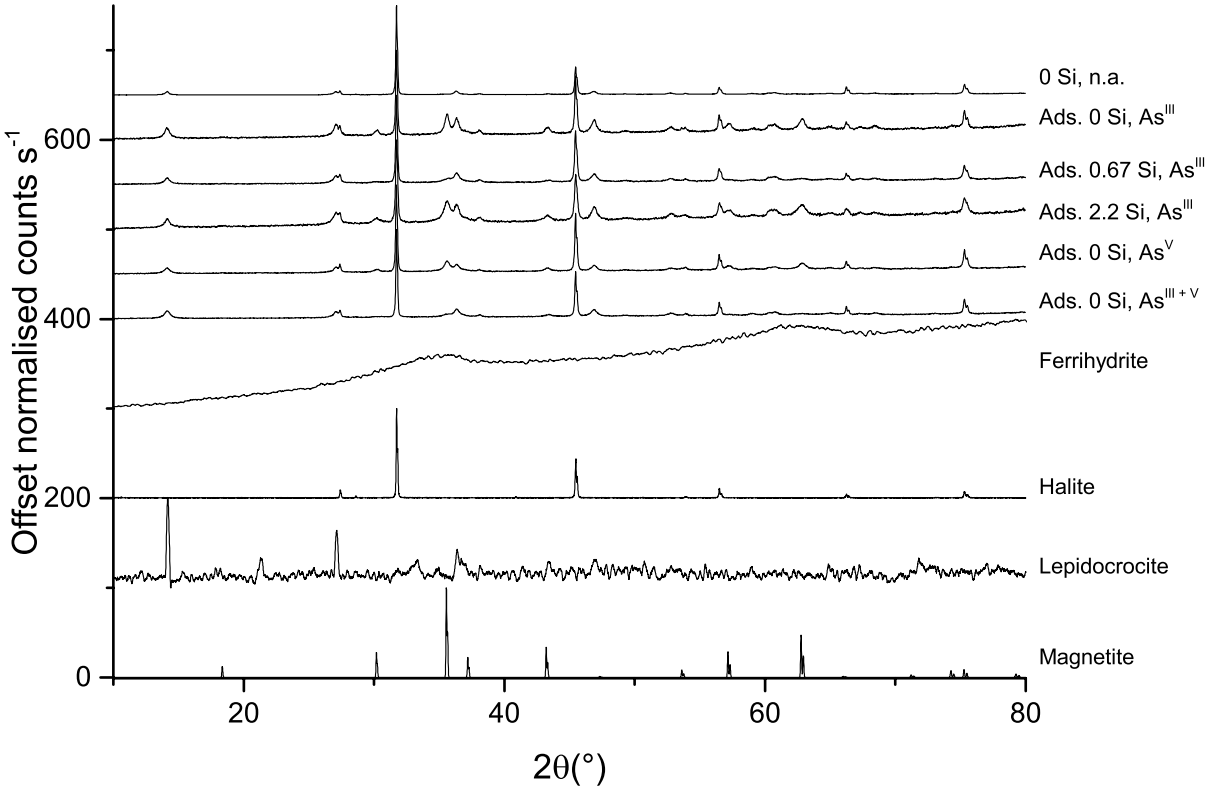

Fig. 1 Examples of PXRD diffractograms. Stacked PXRD spectra of Fe(III)(oxyhydr)oxide precipitate pre-adsorption in 0.0 mM Si (0 Si, n.a.), followed by post-adsorption spectra across the range of Si concentrations 0, 0.67 and 2.2 mM Si and adsorptive treatment. Standard spectra are: 2-line ferrihydrite[24], NaCl (http://rruff.info/halite/display=default/R070292), lepidocrocite (http://rruff.info/Lepidocrocite), and magnetite (http://rruff.info/magnetite/display=default/R061111). All samples have undergone 5 pt signal smoothing, except for 2-line ferrihydrite and lepidocrocite which underwent 30 pt signal smoothing. All spectra have been normalised 0-100.

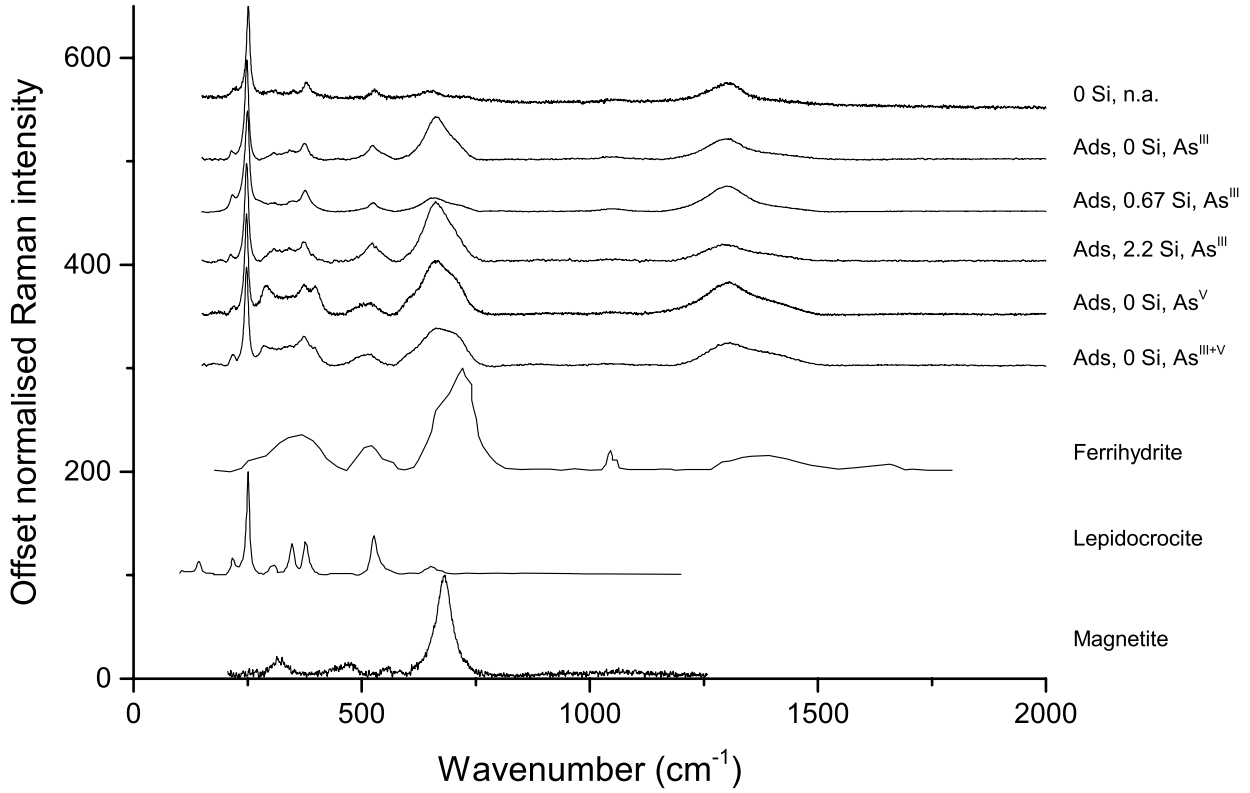

Fig. 2 Examples of selected Raman spectra. Stacked Raman spectra of Fe(III)(oxyhydr)oxide precipitate pre-adsorption in 0.0 mM Si, followed by selected post adsorption spectra across the range of 0, 0.67 and 2.2 mM Si concentrations and different adsorptive treatments. Reference spectra of 2-line ferrihydrite [25], Lepidocrocite[26], and unoriented 785 nm Magnetite (http://rruff.info/magnetite/display=default/R061111).

Table 1: Columns a to c show mineral abundances in Fe(III)(oxyhydr)oxide precipitates, normalised to 1 g total precipitate for adsorption experiments reported in this study (top 6 rows) and from coprecipitation experiments reported in Chi Fru et al. (2016) (bottom 6 rows). Columns d to f show the total adsorption potential[33] of P for each mineral based on the abundances shown in columns a to c. Columns g and h show the total As and P in µmol/g removed from solution during adsorption experiments. Columns i and j show the proportions in % of As and P removed during adsorption compared to that removed during coprecipitation[16]. Columns k and l show hypothetical DIP sorption calculated assuming 100% ferrihydrite in the adsorption experiments. Columns m and n show the proportions in % of As and P removed during adsorption assuming the hypothetical mineralogy of 100% ferrihydrite compared to that removed during coprecipitation experiments[16].

Sample	Mineral abundance (g) in 1 g of sample			P μmol g^{-1} adsorption potential			μmol g^{-1} precipitate		% of Cop		Hypothetical			
											Ads. based on 100% FeH		% of Cop	
	FeH	Lepidocrocite	Magnetite	FeH	Lepidocrocite	Magnetite	As	P	As	P	As	P	As	P
	(a)	(b)	(c)	(d)	(e)	(f)	(g)	(h)	(i)	(j)	(k)	(l)	(m)	(n)
Pre-adsorption, ref	0.28	0.71	0.01	293	87.8	0.3	-	-	-	-	-	-	-	-
Ads. 0 Si, AsIII	0.43	0.16	0.42	441	19.3	14.5	33.8	21.2	9	5	80	50	21	13
Ads. 0.67 Si, AsIII	0.16	0.69	0.15	166	85.7	5.1	4.9	9.3	2	3	31	58	11	20
Ads. 2.2 Si, AsIII	0.46	0.32	0.23	473	39.3	7.8	20.9	4.4	6	1	46	10	12	2
Ads. 0 Si, AsV	0.34	0.39	0.26	355	48.8	9.1	7.0	12.0	7	3	20	35	21	10
Ads. 0 Si, AsIII+V	0.17	0.54	0.29	181	66.5	10.0	30.2	23.6	25	8	173	135	145	49
From Chi Fru et al. 2016														
Cop. 0 Si, AsIII	1.00	-	-	1038	-	-	378	385	-	-	-	-	-	-
Cop. 0.67 Si, AsIII	1.00	-	-	1038	-	-	276	283	-	-	-	-	-	-
Cop. 2.2 Si, AsIII	1.00	-	-	1038	-	-	374	396	-	-	-	-	-	-
Cop. 0 Si, AsV	1.00	-	-	1038	-	-	99.5	365	-	-	-	-	-	-
Cop. 0 Si, AsIII+V	1.00	-	-	1038	-	-	119	279	-	-	-	-	-	-
								Average =	10	4	-	-	42	19
								Std.Dev =	8	2	-	-	52	16

	Adsorption		Coprecipitation	
pH	**Kd**	**Err**	**Kd**	**Err**
5	0.00017	3×10^-05	0.088	0.04
6	0.00029	7×10^-05	0.075	0.09
7	0.00025	2×10^-05	0.063	0.02
8	0.00022	9×10^-05	0.058	0.02
9	0.00018	9×10^-06	0.076	0.05
10	0.00006	3×10^-07	0.071	0.06

Table 2: Mean P distribution coefficients from adsorption experiments (from this study) and coprecipitation experiments (from Chi Fru et al. 2016), averaged from experiments with variable Si levels (0, 0.67 and 2.2 mM) and As speciation (As(III), As(V), and As(III + V)). Errors are shown as standard deviation.

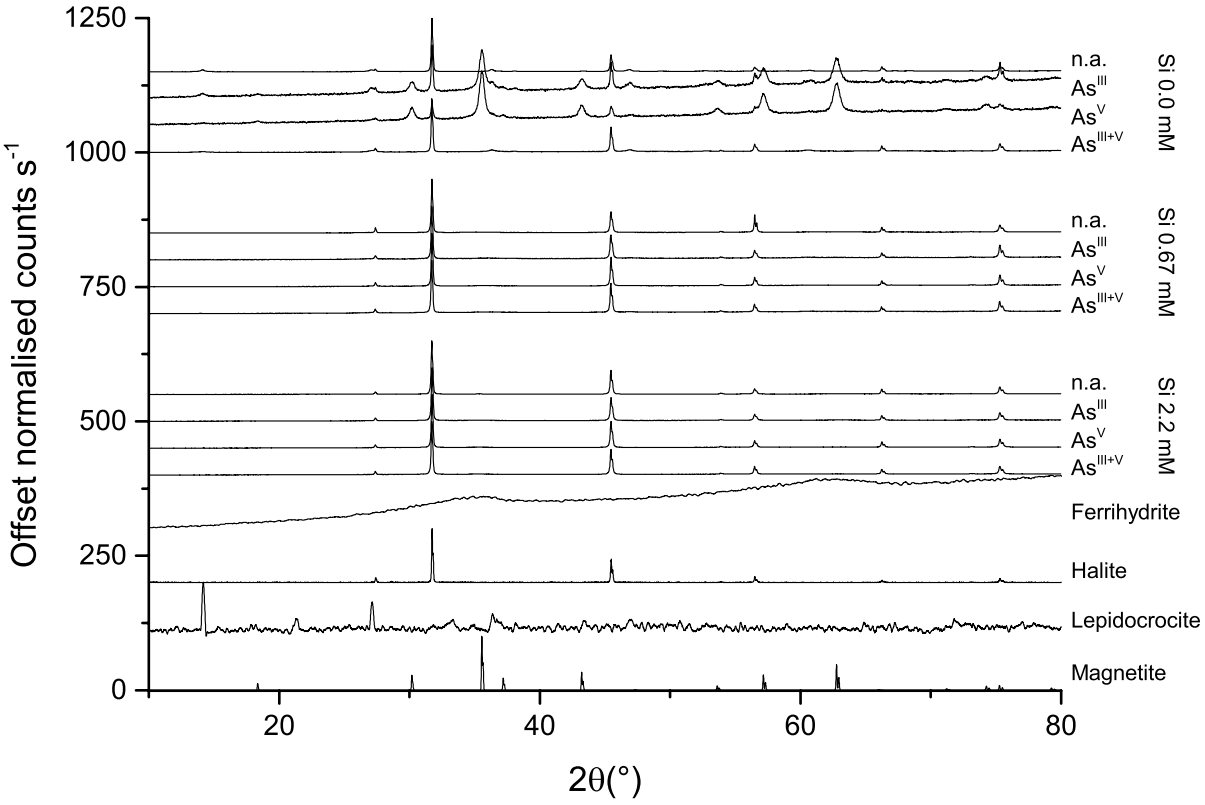

Fig. 3: Examples of PXRD diffractogram. Stacked PXRD spectra of additional Fe(III) (oxyhydr)oxide precipitates synthesised in Si bearing solutions with concentrations of 0, 0.67, and 2.2 mM Si. Pre- adsorption precipitates are denoted as n.a. at each Si concentration, and these are followed by post- adsorption spectra across the range of Si concentrations and experimental treatments. Reference spectra 2- line ferrihydrite[27], NaCl (http://rruff.info/halite/display=default/R070292), lepidocrocite (http://rruff.info/Lepidocrocite), and magnetite (http://rruff.info/magnetite/display=default/R061111). All samples have undergone 5 pt signal smoothing, except for 2-line ferrihydrite and lepidocrocite which underwent 30 pt signal smoothing. All spectra have been normalised 0-100.

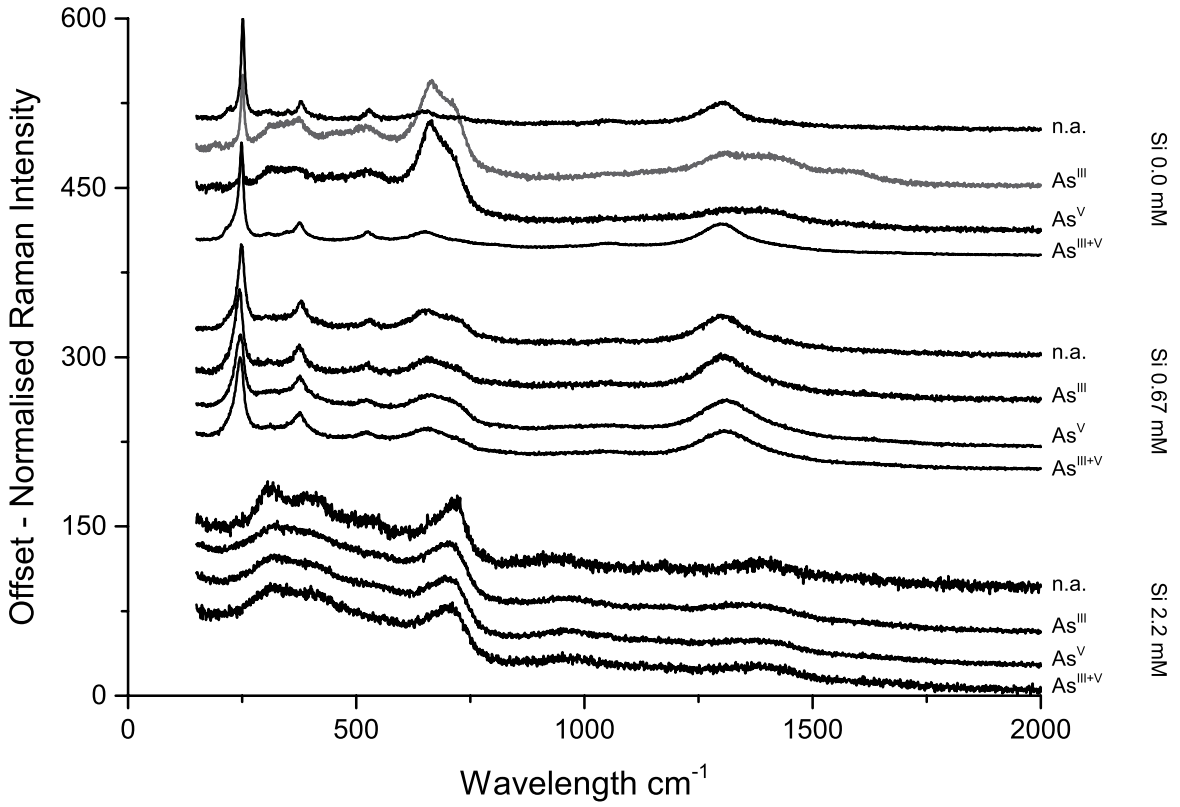

Fig. 4: Stacked Raman spectra of Fe(III)(oxyhydr)oxide precipitates prepared in dissolved Si and exposed to adsorption. Samples denoted n.a. are Fe(III) (oxyhydr)oxide precipitated in 0.0, 0.67 and 2.2 mM Si not exposed to adsorption experiments. Remaining samples from top to bottom represent the adsorptive treatment of P-As(III), P-As(V), P-As(III)-As(V). All samples have undergone 5 pt signal smoothing and have been normalised 0-100.

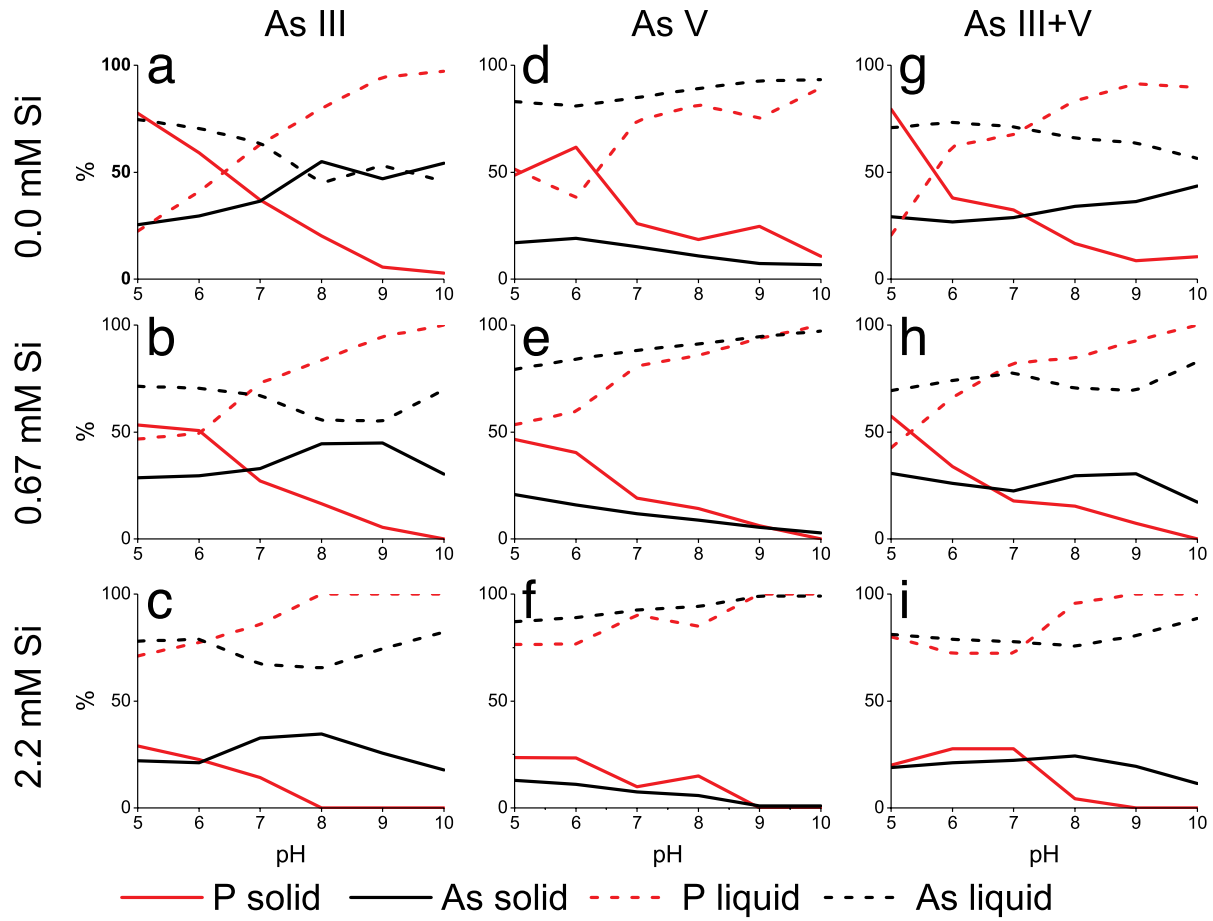

Fig. 5: Distribution of adsorbed P and As after adsorption reactions. Solid lines are P (red) and As (black) adsorbed onto Fe(III)(oxyhydr)oxide precipitates. Dashed lines are P (red) and As (black) remaining in solution. Adsorption reactions are arranged by dissolved Si content and As oxidation state. a-c) As (III) in solution with Si increasing from 0.0 to 2.2 mM Si d-f) As (V) in solution with Si increasing from 0.0 to 2.2 mM Si g-i) As (III+V) in solution with Si increasing from 0.0 to 2.2 mM Si.

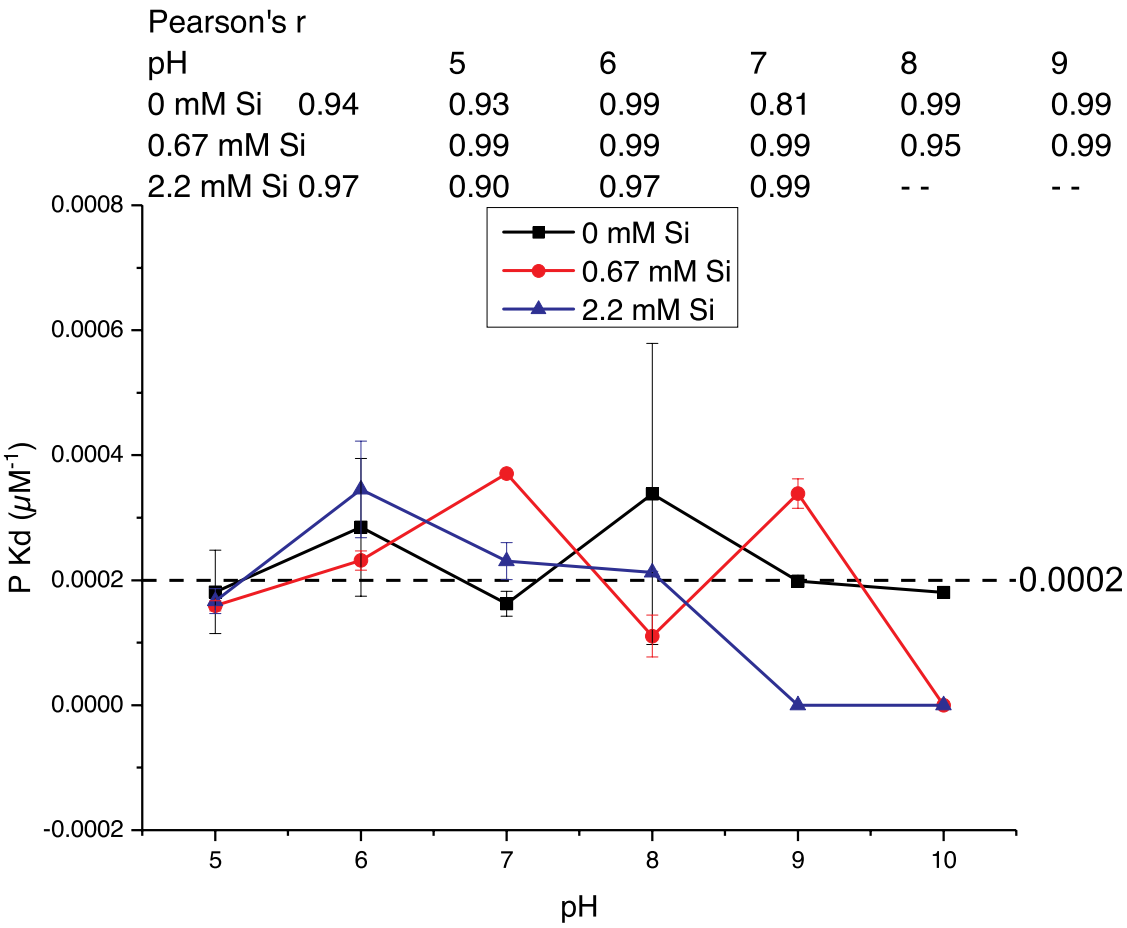

Fig. 6: P distribution coefficients across pH (P-Kd). Calculated P-Kd of P on particles based on the amount adsorbed for reactions in 0.0, 0.67 and 2.2 mM Si. P-Kd is calculated as Molar P/Fe ratio divided by remaining P in solution. Average Kd is displayed by the dashed black line. Error bars are in standard error and Pearson's R-values are for each calculated P-Kd.

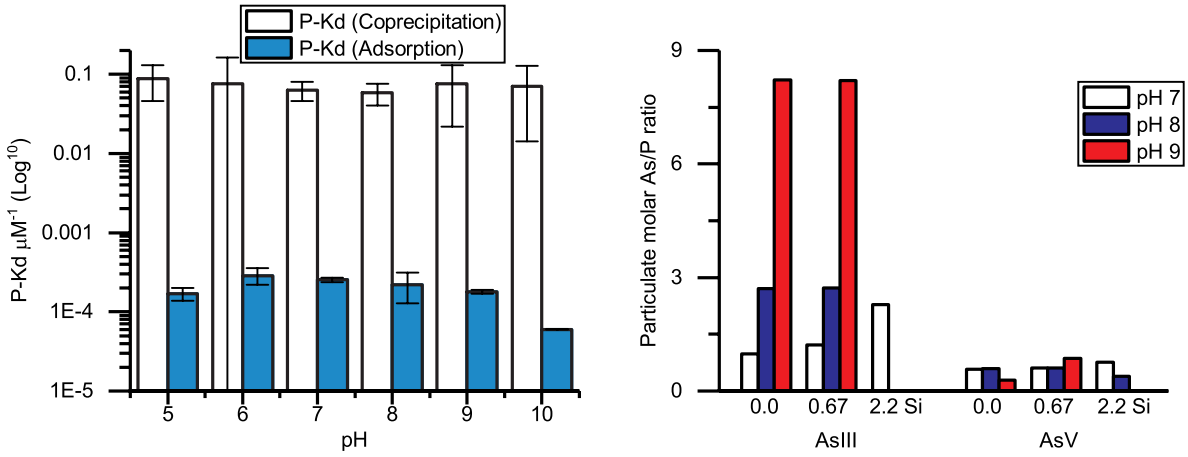

Fig. 7: Particulate As/P ratio and comparison of distribution coefficients between coprecipitation and adsorption. a) Calculated Arsenic uptake relative to phosphate on precipitated Fe(III) (Oxyhydr)oxide particles. b) P distribution coefficients between coprecipitation and adsorption as a function of pH, averaged between tested Si concentrations. White bars, coprecipitation Kd values[16]. Blue bars, adsorption Kd values from this study. Error bars are standard error.

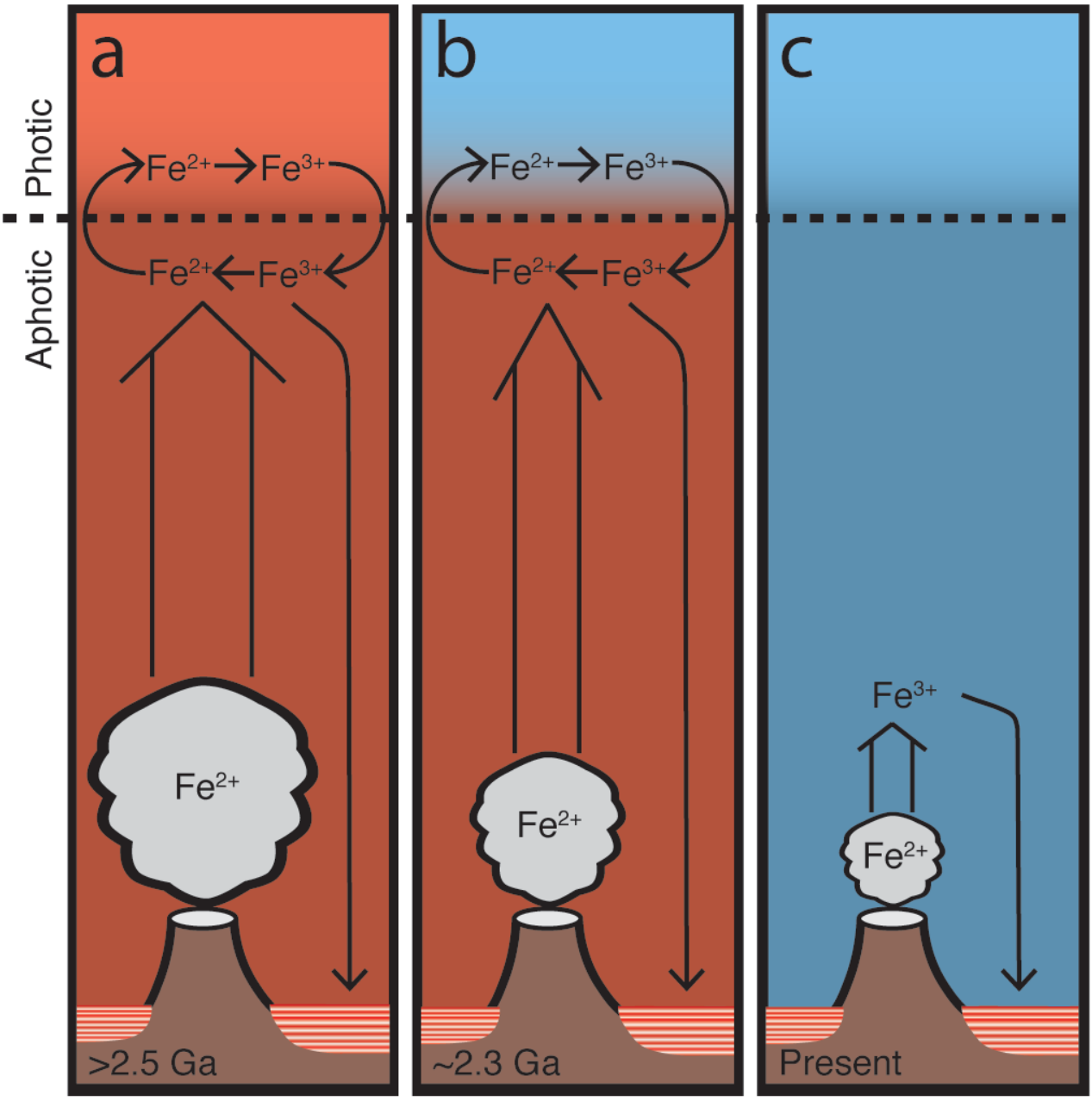

Fig. 8: Conceptual models of redox states of open oceans through Earth's history and the cycling of hydrothermal Fe(II). a) Archean oceans with Fe(II) oxidation to Fe(III) controlled predominantly controlled by photoferrotrophy, but without any clear redoxcline. b) Early Proterozoic oceans with Fe(II) oxidation to Fe(III) intensified by oxidation with molecular O_2 at the ocean surface and microaerobic Fe(II) oxidation in an emergent redoxcline. c) Phanerozoic oceanic cycling of hydrothermal Fe(II) restricted mostly to the deep oceans with markedly reduced hydrothermal activity. Reducing size of hydrothermal plume reflects dropping hydrothermal activity through time[2]. Diagenetic dissimilatory Fe(III) reduction that would have affected the regeneration of Fe(II) from dissolved Fe(III)(oxyhydr)oxides occurs in the sediment as well as the red- coloured water column[1,2,4,14,49,52].

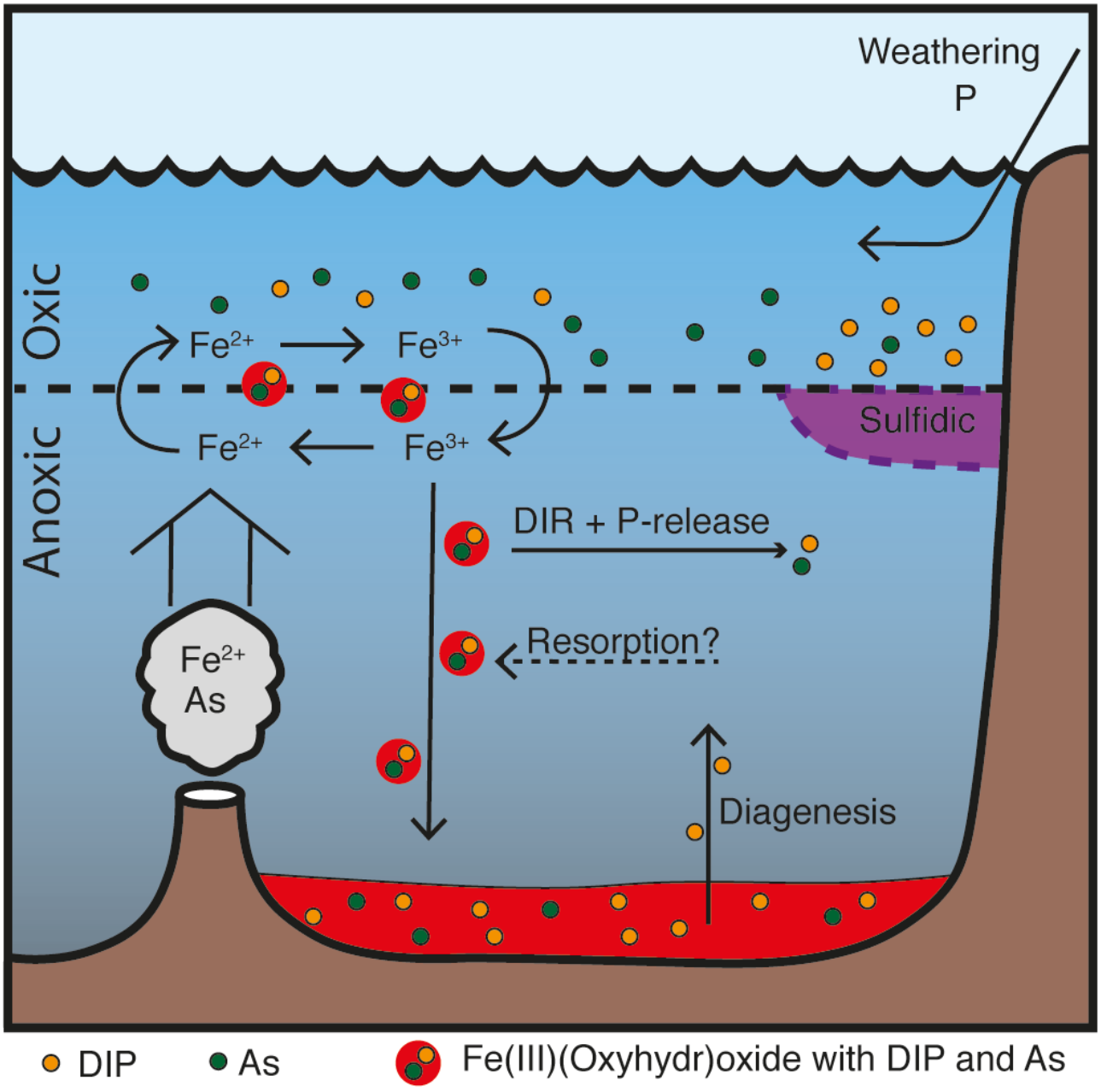

Fig. 9: Conceptual model showing potential P cycling in stratified Early Proterozoic oceans. It is estimated that sulfidic conditions occupied a mere 1-10% of modern seafloor area while pervasive anoxia covered an equivalent of 30-40% of modern seafloor[4]. During coprecipitation P is incorporated into Fe(III)(oxyhydr)oxides when deep anoxic ferruginous waters rise and mix with oxygenated surface waters receiving P from land through riverine delivery of continental weathering. Small amounts of additional P may be bound by ageing Fe(III)(oxyhydr)oxide particles as they sink and are eventually buried. DIR, represents dissimilatory iron reduction, by iron reducing bacteria associated with the oxidation of organic matter, leading to the loss of some P to the water column and regeneration of Fe(II). For simplicity, the effects of Si is not shown in the model.

Supplementary data

Evaluation of uptake mechanisms of phosphate by Fe(III)(oxyhydr)oxides in Early Proterozoic oceanic conditions

Christoffer Hemmingsson, Iain K. Pitcairn, Ernest Chi Fru

Department of Geological Sciences, Stockholm University, SE-10691, Stockholm Sweden

Table 1: Concentrations of As, Fe and P in ppb in the mineral precipitates after adsorption experiments measured by ICP-OES. Starting concentrations in the experimental solutions were 100 μM P and 100 μM As. The relative concentrations of As and P in the supernatant is calculated by subtracting the concentrations in the precipitate from the starting concentrations.

Christoffer Hemmingsson 22/9/17 16:27
Formatted: English (US)

		Precipitate			Precipitate		Supernatant	
Sample	**pH**	**As ppb**	**Fe ppb**	**P ppb**	**As uM**	**P uM**	**As uM**	**P uM**
0 Si. P + AsIII	**5**	189	25100	239	25	78	75	22
0 Si. P + AsIII	**6**	220	22377	182	30	59	70	41
0 Si. P + AsIII	**7**	272	29404	114	37	37	63	63
0 Si. P + AsIII	**8**	409	25420	62	55	20	45	80
0 Si. P + AsIII	**9**	349	27046	18	47	6	53	94
0 Si. P + AsIII	**10**	404	27759	8	54	3	46	97
0 Si. P + AsV	**5**	127	25349	149	17	49	83	51
0 Si. P + AsV	**6**	141	27323	190	19	62	81	38
0 Si. P + AsV	**7**	112	27655	80	15	26	85	74
0 Si. P + AsV	**8**	81	22434	57	11	18	89	82
0 Si. P + AsV	**9**	54	27872	76	7	25	93	75
0 Si. P + AsV	**10**	50	29989	32	7	11	93	89
0 Si. P + AsIII + AsV	**5**	217	29047	244	29	79	71	21
0 Si. P + AsIII + AsV	**6**	198	30324	117	27	38	73	62
0 Si. P + AsIII + AsV	**7**	214	27949	100	29	32	71	68
0 Si. P + AsIII + AsV	**8**	253	28911	51	34	17	66	83
0 Si. P + AsIII + AsV	**9**	269	28371	26	36	9	64	91
0 Si. P + AsIII + AsV	**10**	323	29862	32	43	11	57	89
0.67 Si. P + AsIII	**5**	213	29259	164	29	53	71	47
0.67 Si. P + AsIII	**6**	219	24324	156	29	51	71	49
0.67 Si. P + AsIII	**7**	245	20577	83	33	27	67	73
0.67 Si. P + AsIII	**8**	332	25747	50	45	16	55	84
0.67 Si. P + AsIII	**9**	334	30369	17	45	5	55	95
0.67 Si. P + AsIII	**10**	226	22263	0	30	0	70	100

		Precipitate			Precipitate		Supernatant	
Sample	**pH**	**As ppb**	**Fe ppb**	**P ppb**	**As uM**	**P uM**	**As uM**	**P uM**
0.67 Si. P + AsV	**5**	155	28821	143	21	47	79	53
0.67 Si. P + AsV	**6**	118	23880	124	16	40	84	60
0.67 Si. P + AsV	**7**	87	24453	59	12	19	88	81
0.67 Si. P + AsV	**8**	65	23933	44	9	14	91	86
0.67 Si. P + AsV	**9**	40	28555	19	5	6	95	94
0.67 Si. P + AsV	**10**	20	28938	0	3	0	97	100
0.67 Si. P + AsIII + AsV	**5**	228	29824	176	31	57	69	43
0.67 Si. P + AsIII + AsV	**6**	194	24615	104	26	34	74	66
0.67 Si. P + AsIII + AsV	**7**	167	25556	55	22	18	78	82
0.67 Si. P + AsIII + AsV	**8**	219	24500	47	29	15	71	85
0.67 Si. P + AsIII + AsV	**9**	227	25170	22	31	7	69	93
0.67 Si. P + AsIII + AsV	**10**	128	27724	0	17	0	83	100
2.2 Si. P + AsIII	**5**	163	27711	89	22	29	78	71
2.2 Si. P + AsIII	**6**	156	25241	69	21	23	79	77
2.2 Si. P + AsIII	**7**	243	25824	44	33	14	67	86
2.2 Si. P + AsIII	**8**	258	26364	0	35	0	65	100
2.2 Si. P + AsIII	**9**	190	28323	0	26	0	74	100
2.2 Si. P + AsIII	**10**	133	24700	0	18	0	82	100
2.2 Si. P + AsV	**5**	96	25904	72	13	23	87	77
2.2 Si. P + AsV	**6**	82	22910	72	11	23	89	77
2.2 Si. P + AsV	**7**	56	21180	30	7	10	93	90
2.2 Si. P + AsV	**8**	43	26185	46	6	15	94	85
2.2 Si. P + AsV	**9**	7	28948	0	1	0	99	100
2.2 Si. P + AsV	**10**	6	26474	0	1	0	99	100
2.2 Si. P + AsIII + AsV	**5**	141	25923	62	19	20	81	80
2.2 Si. P + AsIII + AsV	**6**	157	22333	85	21	28	79	72
2.2 Si. P + AsIII + AsV	**7**	166	23494	85	22	28	78	72
2.2 Si. P + AsIII + AsV	**8**	181	27073	13	24	4	76	96
2.2 Si. P + AsIII + AsV	**9**	144	27836	0	19	0	81	100
2.2 Si. P + AsIII + AsV	**10**	85	24333	0	11	0	89	100

Table 2: Concentrations of As, Fe and P in ppb in the mineral precipitates after coprecipitation experiments from Chi Fru et al. (2016). Starting concentrations in the experimental solutions were 100 μM P and 100 μM As. P and As in the precipitate are also presented in μmol liter^{-1} calculated from ICP data. The relative concentrations of As and P in the supernatant is calculated by subtracting the concentrations in the precipitate from the starting concentrations.

Christoffer Hemmingsson 22/9/17 16:27
Formatted: English (US)

		Precipitate			Precipitate		Supernatant	
Sample	**pH**	**As ppb**	**Fe ppb**	**P ppb**	**As uM**	**P uM**	**As uM**	**P uM**
1.0 Fe. 0 Si. P + AsIII	5	39	440	86	4	25	96	75
1.0 Fe. 0 Si. P + AsIII	**6**	38	427	81	4	36	96	64
1.0 Fe. 0 Si. P + AsIII	**7**	739	5103	331	90	100	10	0
1.0 Fe. 0 Si. P + AsIII	8	727	5096	305	91	95	9	5
1.0 Fe. 0 Si. P + AsIII	**9**	735	5287	282	90	84	10	16
1.0 Fe. 0 Si. P + AsIII	**10**	647	5066	153	80	48	20	52
1.0 Fe. 0 Si. P + AsV	5	37	522	97	16	23	95	77
1.0 Fe. 0 Si. P + AsV	**6**	74	755	145	37	42	90	58
1.0 Fe. 0 Si. P + AsV	**7**	211	5578	368	100	100	72	0
1.0 Fe. 0 Si. P + AsV	8	197	5403	353	95	100	73	0
1.0 Fe. 0 Si. P + AsV	**9**	183	5656	283	85	79	75	21
1.0 Fe. 0 Si. P + AsV	**10**	136	5397	57	62	22	82	78
1.0 Fe. 0 Si. P + AsIII + AsV	5	0	0	0	100	100	0	0
1.0 Fe. 0 Si. P + AsIII + AsV	**6**	0	0	0	100	100	0	0
1.0 Fe. 0 Si. P + AsIII + AsV	**7**	0	3	0	100	100	0	0
1.0 Fe. 0 Si. P + AsIII + AsV	8	0	5	0	100	100	0	0
1.0 Fe. 0 Si. P + AsIII + AsV	**9**	40	562	91	95	70	5	30
1.0 Fe. 0 Si. P + AsIII + AsV	**10**	79	892	178	89	38	11	62
1.0 Fe. 0.67 Si. P + AsIII	5	55	879	82	7	26	93	74
1.0 Fe. 0.67 Si. P + AsIII	**6**	134	2037	238	16	77	84	23

		Precipitate			Precipitate		Supernatant	
Sample	**pH**	**As ppb**	**Fe ppb**	**P ppb**	**As uM**	**P uM**	**As uM**	**P uM**
1.0 Fe. 0.67 Si. P + AsIII	**7**	622	5227	294	79	100	21	0
1.0 Fe. 0.67 Si. P + AsIII	8	608	5074	269	77	90	23	10
1.0 Fe. 0.67 Si. P + AsIII	**9**	569	5245	238	72	76	28	24
1.0 Fe. 0.67 Si. P + AsIII	**10**	583	5686	209	64	60	36	40
1.0 Fe. 0.67 Si. P + AsV	5	15	272	26	2	7	98	93
1.0 Fe. 0.67 Si. P + AsV	**6**	111	1852	207	15	62	85	38
1.0 Fe. 0.67 Si. P + AsV	**7**	195	5178	325	26	98	74	2
1.0 Fe. 0.67 Si. P + AsV	8	197	5306	313	27	97	73	3
1.0 Fe. 0.67 Si. P + AsV	**9**	175	5531	267	23	82	77	18
1.0 Fe. 0.67 Si. P + AsV	**10**	149	5295	228	20	69	80	31
1.0 Fe. 0.67 Si. P + AsIII + AsV	5	410	4478	301	55	100	45	0
1.0 Fe. 0.67 Si. P + AsIII + AsV	**6**	423	4685	293	57	100	43	0
1.0 Fe. 0.67 Si. P + AsIII + AsV	**7**	406	4548	258	55	89	45	11
1.0 Fe. 0.67 Si. P + AsIII + AsV	8	322	4183	142	43	54	57	46
1.0 Fe. 0.67 Si. P + AsIII + AsV	**9**	30	653	44	4	15	96	85
1.0 Fe. 0.67 Si. P + AsIII + AsV	**10**	80	1354	139	11	56	89	44
1.0 Fe. 2.2 Si. P + AsIII	5	57	2179	132	7	49	93	51
1.0 Fe. 2.2 Si. P + AsIII	**6**	110	3159	192	14	70	86	30
1.0 Fe. 2.2 Si. P + AsIII	**7**	331	4733	264	43	88	57	12
1.0 Fe. 2.2 Si. P + AsIII	8	326	4886	243	41	79	59	21
1.0 Fe. 2.2 Si. P + AsIII	**9**	315	5006	216	38	64	62	36
1.0 Fe. 2.2 Si. P + AsIII	**10**	253	5086	171	30	50	70	50
1.0 Fe. 2.2 Si. P + AsV	5	395	8728	293	53	60	47	40
1.0 Fe. 2.2 Si. P + AsV	**6**	16	7	0	2	0	98	100
1.0 Fe. 2.2 Si. P + AsV	**7**	164	4833	284	22	95	78	5
1.0 Fe. 2.2 Si. P + AsV	8	161	5203	264	22	78	78	22
1.0 Fe. 2.2 Si. P + AsV	**9**	148	5196	239	20	69	80	31
1.0 Fe. 2.2 Si. P + AsV	**10**	114	5047	198	15	57	85	43
1.0 Fe. 2.2 Si. P + AsIII + AsV	5	403	4530	298	54	100	46	0
1.0 Fe. 2.2 Si. P + AsIII + AsV	**6**	400	4703	300	54	100	46	0

		Precipitate			Precipitate		Supernatant	
Sample	**pH**	**As ppb**	**Fe ppb**	**P ppb**	**As uM**	**P uM**	**As uM**	**P uM**
1.0 Fe. 2.2 Si. P + AsIII + AsV	**7**	365	4794	265	49	88	51	12
1.0 Fe. 2.2 Si. P + AsIII + AsV	8	331	4646	226	44	76	56	24
1.0 Fe. 2.2 Si. P + AsIII + AsV	**9**	59	2008	121	8	43	92	57
1.0 Fe. 2.2 Si. P + AsIII + AsV	**10**	107	3014	204	14	69	86	31
2.0 Fe. 0 Si. P + AsIII	5	55	1043	206	7	68	93	32
2.0 Fe. 0 Si. P + AsIII	**6**	291	2429	316	36	100	64	0
2.0 Fe. 0 Si. P + AsIII	**7**	753	9900	307	97	100	3	0
2.0 Fe. 0 Si. P + AsIII	8	769	10198	302	97	98	3	2
2.0 Fe. 0 Si. P + AsIII	**9**	717	9862	258	95	83	5	17
2.0 Fe. 0 Si. P + AsIII	**10**	771	10969	220	90	62	10	38
2.0 Fe. 0 Si. P + AsV	5	97	1086	206	13	63	87	37
2.0 Fe. 0 Si. P + AsV	**6**	199	7644	321	27	100	73	0
2.0 Fe. 0 Si. P + AsV	**7**	206	10492	327	28	97	72	3
2.0 Fe. 0 Si. P + AsV	8	194	10095	316	26	100	74	0
2.0 Fe. 0 Si. P + AsV	**9**	171	9814	261	23	81	77	19
2.0 Fe. 0 Si. P + AsV	**10**	146	9370	187	20	56	80	44
2.0 Fe. 0 Si. P + AsIII + AsV	5	262	4575	288	35	92	65	8
2.0 Fe. 0 Si. P + AsIII + AsV	**6**	260	4702	274	35	83	65	17
2.0 Fe. 0 Si. P + AsIII + AsV	**7**	215	4576	223	29	69	71	31
2.0 Fe. 0 Si. P + AsIII + AsV	8	180	4772	187	24	55	76	45
2.0 Fe. 0 Si. P + AsIII + AsV	**9**	85	1176	226	11	75	89	25
2.0 Fe. 0 Si. P + AsIII + AsV	**10**	283	2805	313	38	100	62	0
2.0 Fe. 0.67 Si. P + AsIII	5	59	1310	163	7	49	93	51
2.0 Fe. 0.67 Si. P + AsIII	**6**	605	5592	340	72	98	28	2
2.0 Fe. 0.67 Si. P + AsIII	**7**	805	10591	333	97	100	3	0
2.0 Fe. 0.67 Si. P + AsIII	8	770	9920	353	96	98	4	2
2.0 Fe. 0.67 Si. P + AsIII	**9**	757	10761	290	92	85	8	15
2.0 Fe. 0.67 Si. P + AsIII	**10**	275	4325	91	69	45	31	55
2.0 Fe. 0.67 Si. P + AsV	5	48	979	89	7	17	93	83
2.0 Fe. 0.67 Si. P + AsV	**6**	189	6445	307	25	100	75	0

		Precipitate			Precipitate		Supernatant	
Sample	**pH**	**As ppb**	**Fe ppb**	**P ppb**	**As uM**	**P uM**	**As uM**	**P uM**
2.0 Fe. 0.67 Si. P + AsV	**7**	198	9898	319	27	100	73	0
2.0 Fe. 0.67 Si. P + AsV	8	177	9614	280	24	95	76	5
2.0 Fe. 0.67 Si. P + AsV	**9**	124	7009	198	17	81	83	19
2.0 Fe. 0.67 Si. P + AsV	**10**	147	9679	204	20	65	80	35
2.0 Fe. 0.67 Si. P + AsIII + AsV	5	451	9466	315	61	100	39	0
2.0 Fe. 0.67 Si. P + AsIII + AsV	**6**	458	9380	317	61	100	39	0
2.0 Fe. 0.67 Si. P + AsIII + AsV	**7**	428	9159	273	58	89	42	11
2.0 Fe. 0.67 Si. P + AsIII + AsV	8	362	8270	182	49	62	51	38
2.0 Fe. 0.67 Si. P + AsIII + AsV	**9**	53	1168	115	7	41	93	59
2.0 Fe. 0.67 Si. P + AsIII + AsV	**10**	188	2452	272	25	100	75	0
2.0 Fe. 2.2 Si. P + AsIII	5	396	9223	295	35	73	65	27
2.0 Fe. 2.2 Si. P + AsIII	**6**	580	7508	310	73	100	27	0
2.0 Fe. 2.2 Si. P + AsIII	**7**	772	10579	314	93	95	7	5
2.0 Fe. 2.2 Si. P + AsIII	8	710	9944	302	88	96	12	4
2.0 Fe. 2.2 Si. P + AsIII	**9**	662	9794	255	81	83	19	17
2.0 Fe. 2.2 Si. P + AsIII	**10**	592	9916	239	72	68	28	32
2.0 Fe. 2.2 Si. P + AsV	5	25	6	0	3	0	97	100
2.0 Fe. 2.2 Si. P + AsV	**6**	201	7451	321	27	100	73	0
2.0 Fe. 2.2 Si. P + AsV	**7**	200	9874	293	27	100	73	0
2.0 Fe. 2.2 Si. P + AsV	8	172	9414	263	23	96	77	4
2.0 Fe. 2.2 Si. P + AsV	**9**	172	10364	261	23	81	77	19
2.0 Fe. 2.2 Si. P + AsV	**10**	148	10443	226	20	70	80	30
2.0 Fe. 2.2 Si. P + AsIII + AsV	5	438	9285	312	59	100	41	0
2.0 Fe. 2.2 Si. P + AsIII + AsV	**6**	419	8827	296	56	100	44	0
2.0 Fe. 2.2 Si. P + AsIII + AsV	**7**	410	9033	266	55	91	45	9
2.0 Fe. 2.2 Si. P + AsIII + AsV	8	366	9131	208	49	69	51	31
2.0 Fe. 2.2 Si. P + AsIII + AsV	**9**	82	2596	170	11	58	89	42
2.0 Fe. 2.2 Si. P + AsIII + AsV	**10**	329	6348	303	44	100	56	0